α-conjugate neck structures in the collisions of 35 MeV/nucleon ^{40}Ca with ^{40}Ca

K. Schmidt,[1,2,*] X. Cao,[3,1] E. J. Kim,[1,4] K. Hagel,[1] M. Barbui,[1] J. Gauthier,[1] S. Wuenschel,[1] G. Giuliani,[1,5] M. R. D. Rodrigues,[1,6] H. Zheng,[1,5] M. Huang,[1,7] N. Blando,[1] A. Bonasera,[1,5] R. Wada,[1] C. Botosso,[1] G. Liu,[3] G. Viesti,[8] S. Moretto,[8] G. Prete,[9] S. Pesente,[8] D. Fabris,[8] Y. El Masri,[10] T. Keutgen,[10] S. Kowalski,[2] A. Kumar,[11] G. Zhang,[1,3] and J. B. Natowitz[1]

[1]*Cyclotron Institute, Texas A&M University, College Station, Texas 77843, USA*
[2]*Institute of Physics, University of Silesia, 40-007 Katowice, Poland*
[3]*Shanghai Institute of Applied Physics, Chinese Academy of Sciences, Shanghai 201800, China*
[4]*Division of Science Education, Chonbuk National University, Jeonju 561-756, Korea*
[5]*Laboratori Nazionali del Sud, INFN, via Santa Sofia, 62, 95123 Catania, Italy*
[6]*Instituto de Física, Universidade de São Paulo,Caixa Postal 66318, CEP 05389-970, São Paulo, SP, Brazil*
[7]*College of Physics and Electronics information, Inner Mongolia University for Nationalities, Tongliao, 028000, China*
[8]*Dipartimento di Fisica dell'Università di Padova and INFN Sezione di Padova, I-35131 Padova, Italy*
[9]*INFN Laboratori Nazionali di Legnaro, I-35020 Legnaro, Italy*
[10]*Universite Catholique de Louvain, B-1348 Louvain-la-Neuve, Belgium*
[11]*Nuclear Physics Laboratory, Department of Physics, Banaras Hindu University, 221005 Varanasi, India*

(Received 2 December 2016; published 30 May 2017)

The deexcitation of alpha-conjugate nuclei produced in reactions of 35 MeV/nucleon ^{40}Ca with ^{40}Ca has been investigated. Particular emphasis is placed on examining the dynamics of collisions leading to projectile-like fragment exit channels. A general exploration of the reaction systematics reveals the binary dissipative character of the collisions and a hierarchy effect similar to that seen for heavier systems. Investigation of the subset of events characterized by a total α-conjugate mass (α particles plus α-conjugate fragments) equal to 40 and atomic number equal to 20 reveal a dominance of α-conjugate exit channels. The hierarchy effect for these channels leads to the production of α-clustered neck structures with potentially exotic geometries and properties.

DOI: 10.1103/PhysRevC.95.054618

I. INTRODUCTION

Nuclei are normally treated as consisting of fermions. However, in-medium correlations and the strong binding of the α particle can lead to situations in which an α cluster picture can be employed to understand nuclear structure and decay properties [1–4]. Both theoretical calculations and experimental observations provide strong support for the α-clustered nature of light α-conjugate (even-even $N = Z$) nuclei [5–7]. Loosely bound states with excitation energies near the alpha emission thresholds states may be a manifestation of the tendency of low-density low-temperature nuclear matter to undergo Bose condensation [8–12]. For example, the 7.65 MeV Hoyle state in ^{12}C, important for the solar 3α capture process [13] is known to possess a large radius [14], which could allow the α particles to retain their quasifree characteristics.

The role of α clusters in reaction dynamics is itself an interesting topic. Cluster effects are often seen in transfer reactions involving light nuclei [15]. Studies of more violent collisions of α conjugate nuclei might reveal important effects of these correlations on the collision dynamics and in determination of the reaction exit channels. Given that near-Fermi-energy nuclear collisions can drastically modify the temperatures, densities, and cluster properties of nucleonic matter, the possibility that short-lived Bose condensates might be fleetingly produced in such collisions is an intriguing idea. Recently the emission of three α from the Hoyle state has been characterized for ^{12}C produced in several different reactions [16–19]. Results for the ratio of simultaneous to sequential deexcitation differ and the influence of medium or proximity effects on the deexcitation modes of that state in complex reactions remains an open question. The authors of Ref. [20] have argued that enhanced α emission occurs during the thermal expansion of ^{20}Ne, ^{20}Ne, and ^{24}Mg projectile-like fragments produced in 25 MeV/nucleon, ^{40}C + ^{12}C collisions, reflecting the α-conjugate nature of the parent fragments. Signatures of and possible evidence for Bose–Einstein condensation and Fermi quenching in the decay of hot nuclei produced in 35MeV/nucleon ^{40}+C^{40}C collisions have been discussed in Refs. [21–23]. Evidence of cluster effects in the dynamics at much higher energies were reported in Ref. [24].

To pursue the question of the effects of α-like correlations and clustering in collisions between α-conjugate nuclei we have embarked on a program of experimental studies of such collisions at and below the Fermi energy by using the Neutron Ion Multidetector for Reaction Oriented Dynamics with the Indiana Silicon Sphere (NIMROD-ISiS) array at Texas A&M University [25]. A dominating α-clustered nature of the colliding matter could manifest itself in the kinematic properties and yields of the α-conjugate products. While the granularity of our detection system is not sufficient for high-resolution fragment and particle correlations, we are able to explore certain features of the reactions which lead to large cross sections for α-conjugate reaction products.

*katarzyna.schmidt@us.edu.pl

In this paper we report results for a study of α clusterization effects in midperipheral collisions of $^{40}C + ^{40}C$ at 35 MeV/nucleon. We first present some global observations and then focus on collisions in which excited projectile-like fragments disassemble into α-conjugate products.

II. EXPERIMENTAL DETAILS

The experiment was performed at Texas A&M University Cyclotron Institute. ^{40}Ca beams produced by the $K500$ superconducting cyclotron impinged on ^{40}Ca targets at the energy of 35 MeV/nucleon. The reaction products were measured by using a 4π array, NIMROD-ISiS [25] which consisted of 14 concentric rings covering from 3.6° to 167° in the laboratory frame. In the forward rings with $\theta_{lab} \leqslant 45°$, two special modules were set having two Si detectors (150 and 500 μm) in front of a CsI(Tl) detector (3–10 cm), referred to as supertelescopes. The other modules (called telescopes) in the forward and backward rings had one Si detector (one of 150, 300, or 500 μm) followed by a CsI(Tl) detector. The pulse shape discrimination method was employed to identify the light charged particles with $Z \leqslant 3$ in the CsI(Tl) detectors. Intermediate mass fragments (IMFs), were identified with the telescopes and supertelescopes by using the "ΔE-E" method. In the forward rings an isotopic resolution up to $Z = 12$ and an elemental identification up to $Z = 20$ were achieved. In the backward rings only Z = 1–2 particles were identified, because of the detector energy thresholds. In addition, the neutron ball surrounding the NIMROD-ISiS charged particle array provided information on average neutron multiplicities for different selected event classes. Further details on the detection system, energy calibration, and neutron ball efficiency can be found in Refs. [25–27].

It is important to note that, for symmetric collisions in this energy range, the increasing thresholds with increasing laboratory angle lead to a condition in which the efficiencies strongly favor detection of projectile-like fragments from midperipheral events. The modeling of these collisions by using an antisymmetrized molecular dynamics (AMD) code [28,29] coupled with the statistical code GEMINI [30] as an afterburner and applying the experimental filter demonstrates that this is primarily an effect of energy thresholds.

III. GENERAL CHARACTERIZATION OF THE REACTIONS

Our previous study of the $^{40}C + ^{40}C$ at 35 MeV/nucleon focused on the multifragment exit channels and led to the conclusion that even the most violent and most central collisions were binary in nature [31]. Similar conclusions on the dominant binary nature of reactions with 35 MeV/nucleon ^{24}Mg projectiles were reported by Larochelle *et al.* [32].

We initiated the present analysis of the new data by reconstructing the "initial apparent excitation energy" E^* of the projectile-like fragments through calorimetry. E^* was defined as the sum, for accepted particles, of the particle kinetic energies in the frame of the total projectile-like nucleus (determined by reconstruction of the mass and velocity of the primary excited nucleus from its deexcitation products), minus

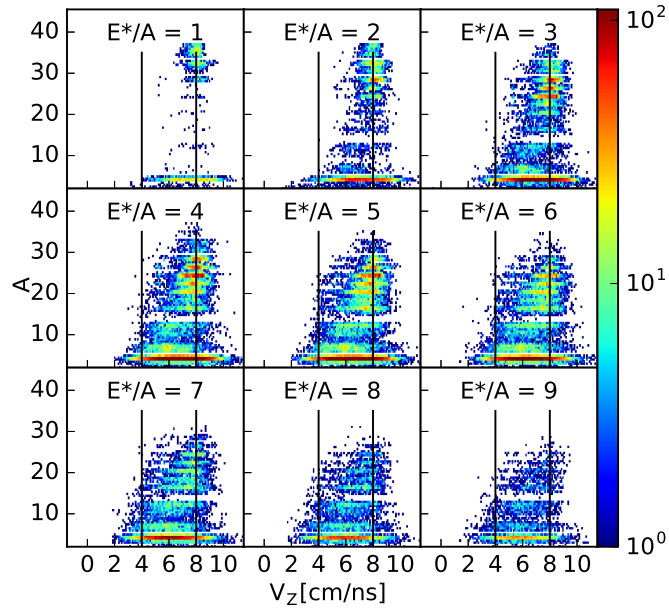

FIG. 1. Yields of the three heaviest fragments in the event as a function of the fragment parallel velocity in different windows of initial apparent excitation energy E^*/A. The projectile velocity is 8.0 [cm/ns]. The c.m. velocity is 4.0 [cm/ns].These two velocities are indicated by vertical lines in each panel.

the reaction Q value. See Eq. (1):

$$E^* = \sum_{i=1}^{M} K_{cp}(i) + M_n\langle K_n\rangle - Q. \quad (1)$$

Here M is the total charged particle multiplicity, $K_{cp}(i)$ is the source frame kinetic energy of charged particle i, M_n is the average neutron multiplicity, $\langle K_n\rangle$ is the average neutron kinetic energy, and Q is the disassembly Q value. For this purpose the average kinetic energy of the neutrons was taken to be equal to the average proton kinetic energy with a correction for the Coulomb barrier energy. Average neutron multiplicities were determined by applying efficiency corrections to the average neutron multiplicities observed with the neutron ball [27]. For a compound nucleus this initial apparent excitation energy would correspond to the energy available for statistical decay of the primary nucleus. We caution that, given the binary nature of the collisions studied, the deexciting projectile-like nucleus is not necessarily a fully equilibrated nucleus. Nevertheless, this measure of energy deposition into the systems studied can serve as a useful sorting parameter. For the initial event selection we included all particles and fragments detected in an event. As will be seen, this event selection is revised in subsequent sections where we employ a more restrictive filtering to derive excitation energies.

In Fig. 1 the mass numbers A of the three heaviest fragments in each event are plotted against their laboratory-frame parallel velocities for 1 MeV increments in E^*/A. The favored detection of projectile-like species for all windows is clearly seen in this figure. Most of the fragments have velocities above the center-of-mass velocity, 4.0 [cm/ns]. Increasing excitation

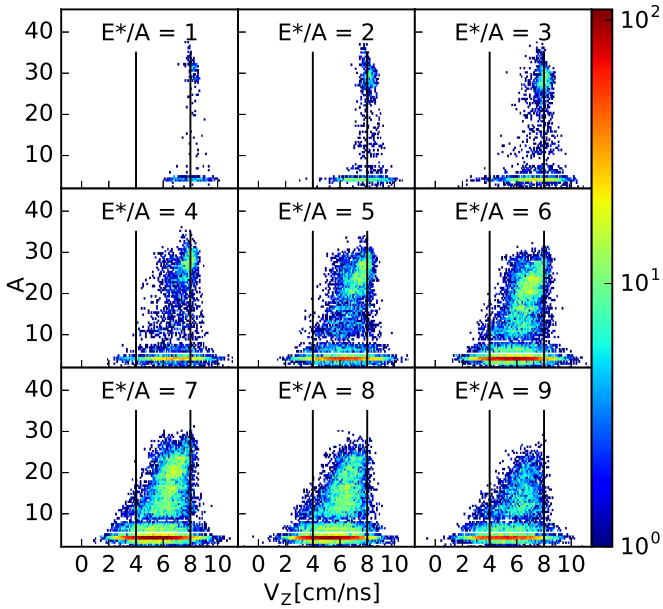

FIG. 2. Filtered AMD-GEMINI results, similar as Fig. 1.

energy corresponds, at least qualitatively, to decreasing impact parameter and increased collision violence. This is manifested in the figure by the decrease in yields of the heaviest mass products and increasing yields of lighter mass products as excitation increases. At low excitation energies the majority of the heavier products have parallel velocities near the beam velocity of 8.0 [cm/ns]. The similar mean laboratory velocities suggest that the lighter fragments are produced in by statistical deexcitation of the initial projectile-like fragment. As the excitation energy increases, a clear correlation between parallel velocity and fragment mass is observed. For these excitations, corresponding to the region of midperipheral collisions, the parallel velocity decreases as the fragment mass decreases. This trend could reflect a greater degree of energy dissipation with decreasing impact parameter and/or the onset of neck emission [33–35]. We shall return to this question.

Figure 2 shows the results of AMD-GEMINI calculations for this 35 MeV/nucleon $^{40}C + ^{40}C$ system filtered by using our experimental geometries and thresholds. The AMD calculation [28,29] followed the reaction until 300 fm/c after the collision. The code GEMINI [30] was employed as an afterburner to deexcite the primary fragments. We note that the plots in Fig. 2 look qualitatively similar to those in Fig. 1. However, at the lower excitation energies the AMD exhibit narrower velocity distributions and different yield distributions. This may be a manifestation of more transparency in the AMD collision than in the experiment [36].

IV. SELECTION OF $A = 40$, $Z = 20$ PROJECTILE-LIKE SOURCE

Our previous analyses of near-Fermi-energy collisions [26,27] indicate that significant proton emission occurs in the earliest stages of the collision as the nucleon momentum distributions are thermalizing, not in the later stage disassembly. To better characterize the source of the light particles in the selected events we explored the $Z = 1$ and $Z = 2$ light particle emission by carrying out both two-source and three-source fits assuming that the observed light charged particle emission can be attributed to primary sources moving in the laboratory frame, a projectile-like source (PLF), a target-like source (TLF), and a (virtual) intermediate velocity source (IV) moving at a velocity $\sim\frac{1}{2}$ the projectile velocity [37]. This latter source reflects nucleon-nucleon collisions occurring early in the process. In each source frame the emission was assumed to have a Maxwellian distribution and each of the sources is described by a source velocity, temperature, Coulomb barrier, and particle multiplicity [26]. A comparison of the total yields with those obtained from the source fits to the proton energy spectra indicates the proton emission is low, with average multiplicities $\sim$2 and is dominated by emission from an intermediate velocity source having an apparent velocity of $\sim\frac{1}{2}$ that of the projectile rather than from later statistical deexcitation. For this light symmetric system we expect the same to be true for the neutrons. While the neutron kinetic energies are not accessible in this experiment, the efficiency corrected neutron multiplicities obtained by using the neutron ball are similar to the proton multiplicities.

For d and t emission the average multiplicities are much lower and about half the particles are emitted from the IV source. The ^{3}He emission was too low to allow reasonable fits. To pursue our analysis we focus on events for which $A = 40$ and $Z = 20$. However, in this selection we have neglected both protons and neutrons.

V. TESTS OF STATISTICAL BEHAVIOR

Horn and coworkers suggested that the ratio of average excitation energy to the average exit channel separation energy could be used as a test for statistical emission from highly excited lighter nuclei [32–35,37,38]. For their model assumptions regarding a Fermi gas level density, negligible emission barriers and a linear increase of available exit channels with increasing excitation energy, they concluded that the ratio should be constant with a value near two. They also concluded that the statistical variance of this ratio would be small enough to enable this ratio to be used as an identifier of statistical deexcitation on an event-by-event basis [38]. Experimental observations of constant values of the ratio have been cited as evidence for strong dominance of statistical deexcitation of projectile-like fragments [32–35,37,38]. In Fig. 3 we present, for all observed PLF exit channels with 10 or more events having $A = 40$ and $Z = 20$ (not including n or p as discussed above), a plot of average excitation energy E^* vs exit channel separation energy $-Q$. In general these data are similar to previous results [32,38,39]. A linear fit to these data leads to a slope parameter of 2.39. This result, well above two, is close to that extracted in Ref. [32]. Based on comparisons with statistical model results the authors of Ref. [32] concluded that there are important dynamic effects in midperipheral and central reactions at 35 MeV/nucleon and above. A closer investigation of Fig. 3 indicates that some prominent channels, particularly at lower separation energies, have ratios well above the average values. This observed deviation suggests

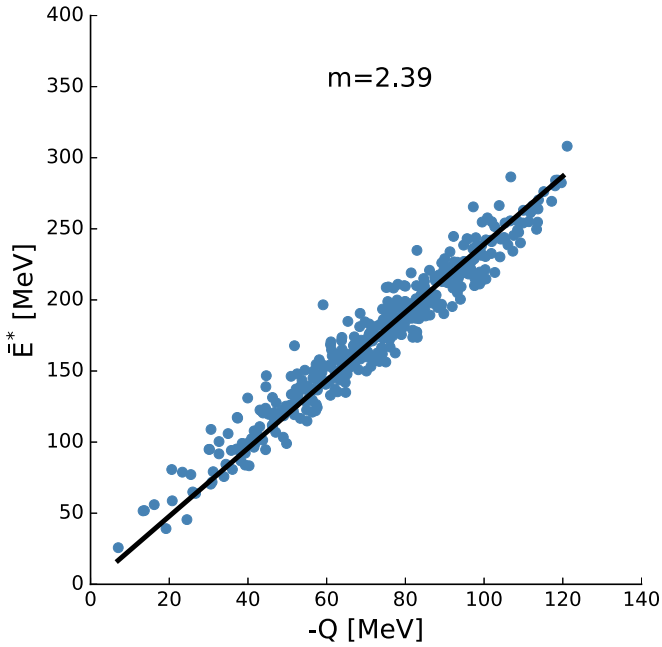

FIG. 3. Average excitation energy vs exit channel separation energy for the deexcitation channels of $A = 40$, $Z = 20$ nuclei selected as described in the text. Data are represented by small filled dots. The linear least squares fit to the data is represented by the solid line.

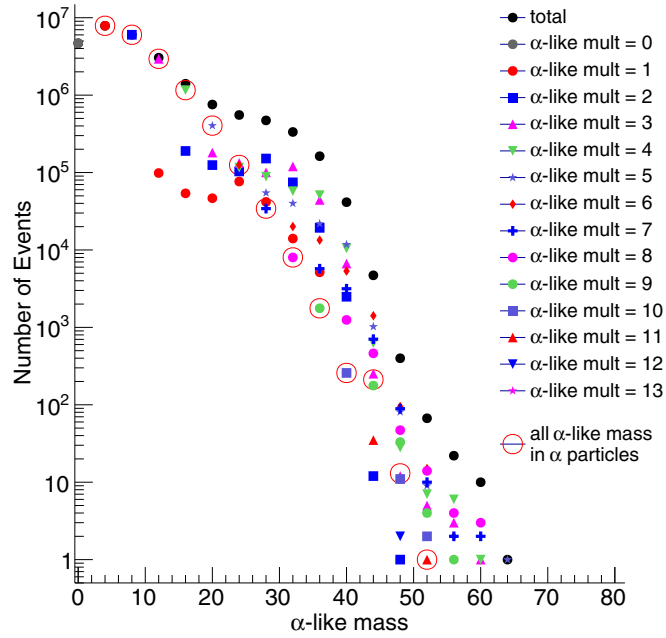

FIG. 4. Detected number of events yielding α particles or α-conjugate nuclei in the collision of ^{40}Ca with ^{40}Ca at $35A$ MeV, plotted against total detected mass of α-conjugate nuclei. Small filled circles represent total yields. Open circles represent yields for events in which only α particles contribute to the A_L.

that these reactions warrant additional exploration. We return to these results in the Sec. VII.

VI. ALPHA-CONJUGATE EXIT CHANNELS

The main purpose of the present study was to explore exit channels composed of α particles or α-conjugate nuclei. To focus on such channels, the event-by-event data were sorted as a function of the total detected "α-like mass" A_L, i.e., the sum of the masses of the detected products that are either α particles or α-conjugate nuclei. Figure 4 depicts the resultant event yields. For a given total α-like mass, several different decay channels are often possible. Events for which all of the detected α conjugate mass is in α particles are indicated by the large open circles in Fig. 4. A total α-like mass as large as 85% of the entrance channel mass is seen, but with very low statistics. The shoulder in the α-like mass ~ 40 region and rapid decrease beyond that reflects the detector selectivity for projectile-like fragments from midperipheral events.

VII. ALPHA-CONJUGATE $A_L = 40$ EXIT CHANNELS

For the analyses which follow we have chosen to focus on those events for which $A_L = 40$ and compare the properties of the 19 possible exit channels for the disassembly of the ^{40}Ca nucleus into α particles or α-conjugate nuclei. The 19 possible combinations of α-conjugate nuclei which satisfy this total α-conjugate mass $= 40$ criterion are schematically indicated in Fig. 5. This depiction is similar to that of the Ikeda diagram which is commonly invoked in discussions of the cluster structure of light nuclei [40]. The events selected typically have a few $Z = 1$ particles (and neutrons) and, in rare cases, a heavier non-α-conjugate fragment, associated with them. To further refine our event selection we exclude the fraction of the $A_L = 40$ events (11%) with non-α-conjugate fragments from the analysis. In our selection we have allowed $Z = 1$ particles and neutrons but we have redetermined the excitation energies by excluding the $Z = 1$ particles and

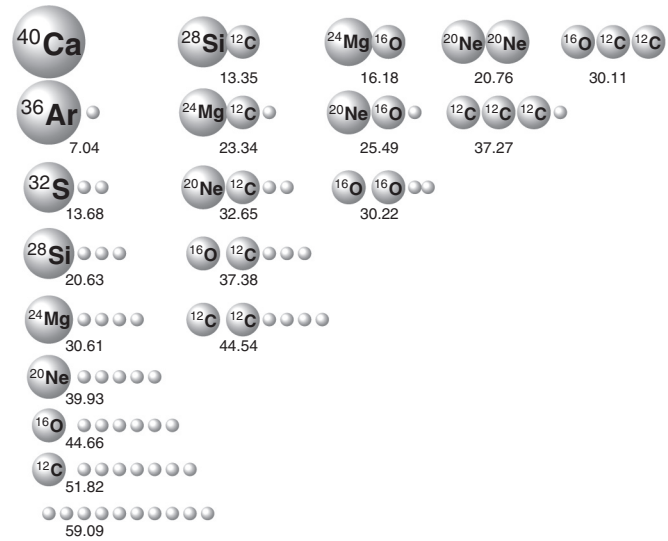

FIG. 5. Ikeda-like diagram for the possible α-conjugate components of ^{40}Ca. Separation energy $-Q$ in MeV for each decay channel is shown.

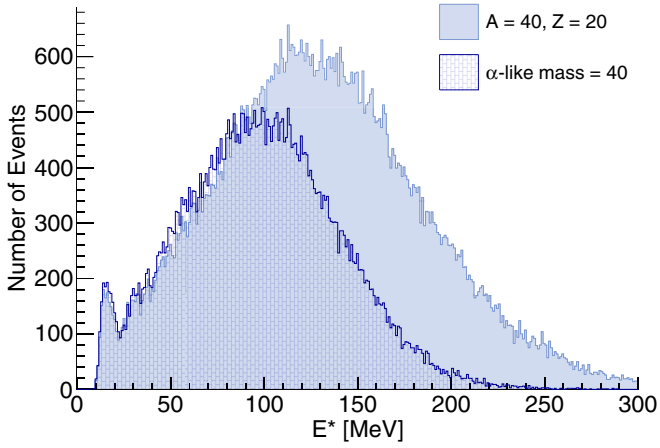

FIG. 6. Excitation energy distributions for $A = 40$, $Z = 20$ derived as indicated in the text. The blue area represents the data for all such events. The hatched area represents the data for $A_L = 40$ events.

neutrons because they are primarily pre-equilibrium particles, representing energy dissipation but not energy deposition into the PLF [41]. This leads to slightly smaller excitation energies and introduces a small uncertainty. As invariant velocity plots for the α particles indicate that a small fraction of the α particles may result from pre-equilibrium emission or from the target-like source, α particles with PLF source frame energies greater than 40 MeV were also excluded to remove those contributions. The excitation energy distributions derived for all $A = 40$, $Z = 20$ PLF events defined in this manner are presented in Fig. 6. The $A_L = 40$ events account for 61% of the $A = 40$, $Z = 20$ PLF events detected. Detected events with α-conjugate mass $= 40$ account for to 0.23% of the total experimental events collected. Filtered AMD calculations predict about half that amount, 0.11%. In Fig. 7 the excitation functions for the different $A_L = 40$ exit channels detected in this reaction are presented. The distribution of yields in the different exit channels are presented in Fig. 8 as percentages of the total $A_L = 40$ yields. Both the experimental results and those from the filtered AMD-GEMINI calculation are presented. They both suggest that the most probable decay modes are those with one heavy α-like mass fragment and several α particles in the exit channel. While the two distributions are similar, there are some significant differences between the experimental and calculated results. In Fig. 9 we plot, for each identified exit channel of the decay of the selected $A = 40$, $Z = 20$ nuclei, the fractional yield vs the ratio of average excitation energy to exit channel separation energy (see Fig. 3). Results are presented for both the experimental data (top) and AMD simulation (bottom). Each exit channel is represented by a solid circle. We have further identified the $A_L = 40$ exit channels by using open diamonds. We see that, in both frames of Fig. 9, these channels are those with the largest values of $E^*/-Q$ from the systematics. Their ratios are well above the values for the other channels with similar separation energies and in general their yields are quite high. An exploration of other high-yield channels reveals that these are generally channels in which the deviations from $A_L = 40$ reflect the existence of deuterons or ^{6}Li nuclei in the exit channel. These are exit channels, such as, for example, (^{30}P,2α,d), (^{26}Al,3α,d), (^{22}Na,4α,d), and (^{22}Na,^{6}Li,3α). We identify such channels with additional open circles around the solid circles. These channels might well be those in which an initial breakup into α particles and/or α-conjugate fragments is followed by a secondary emission or breakup. If so, the fraction of initial α-conjugate breakups of $A = 40$, $Z = 20$ nuclei is much larger than the 61% observed in Fig. 6. The excitation energy evolution of Figs. 1 and 2 suggest that it is the dynamic evolution which favors the extension of these excitation functions to higher energies and shifts the ratios higher. The degree to which this large fraction of α-conjugate deexcitations reflects the initial α-conjugate nature of ^{40}Ca or the dynamic evolution of the excitation and density warrants further investigation.

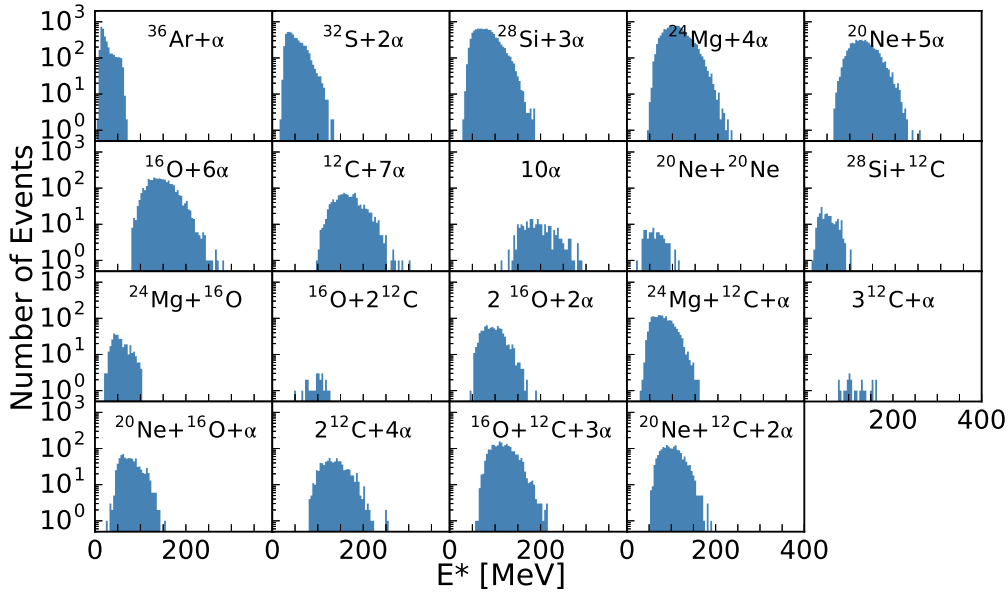

FIG. 7. Excitation functions for the $A_L = 40$ events discussed in the text.

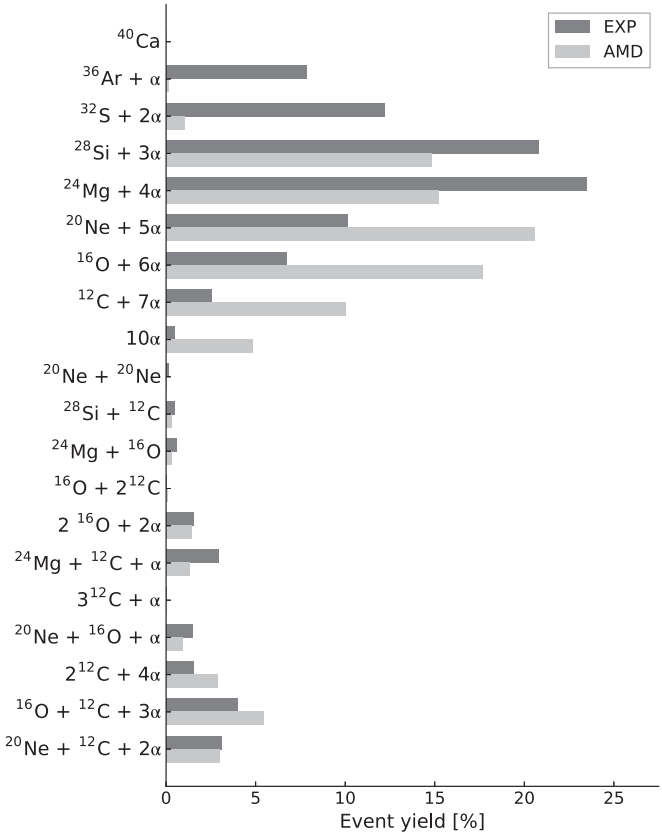

FIG. 8. Percentages of $A_L = 40$ events appearing in the possible exit channels. The experimental results are represented by solid dark grey bars. The filtered AMD-GEMINI results are represented by solid silver bars.

VIII. COLLISION DYNAMICS FOR $A_L = 40$

To more explicitly probe the dynamics of the $A_L = 40$ events we have constructed momentum space representations of the correlations among exit channel products using sphericity and coplanarity to characterize the event shapes [42,43]. Sphericity S and coplanarity C are defined as

$$S = \frac{3}{2}\frac{\lambda_1 + \lambda_2}{\lambda_1 + \lambda_2 + \lambda_3}, \tag{2}$$

$$C = \frac{\sqrt{3}}{2}\frac{\lambda_2 - \lambda_1}{\lambda_1 + \lambda_2 + \lambda_3}, \tag{3}$$

where the λ are the eigenvalues of the flow tensor in the c.m. of the source system and are ordered so that $\lambda_1 < \lambda_2 < \lambda_3$. A combined plot of S and C reveals the dominant shape in momentum space.

The upper left panel of Fig. 10 provides a schematic representation of the interpretation of momentum space distributions using these coordinates. Events at 0.0, 0.0 are rod like. Those at 0.75, 0.43 are disk like. Events along the line between these points are coplanar. The events at 1.0, 0.0 are spheres. Oblate and prolate shapes will appear in the regions between these extremes. It is important to note that the shapes in the sphericity-coplanarity plots do not reflect the actual geometric shape of the decaying nuclei but represent the shape

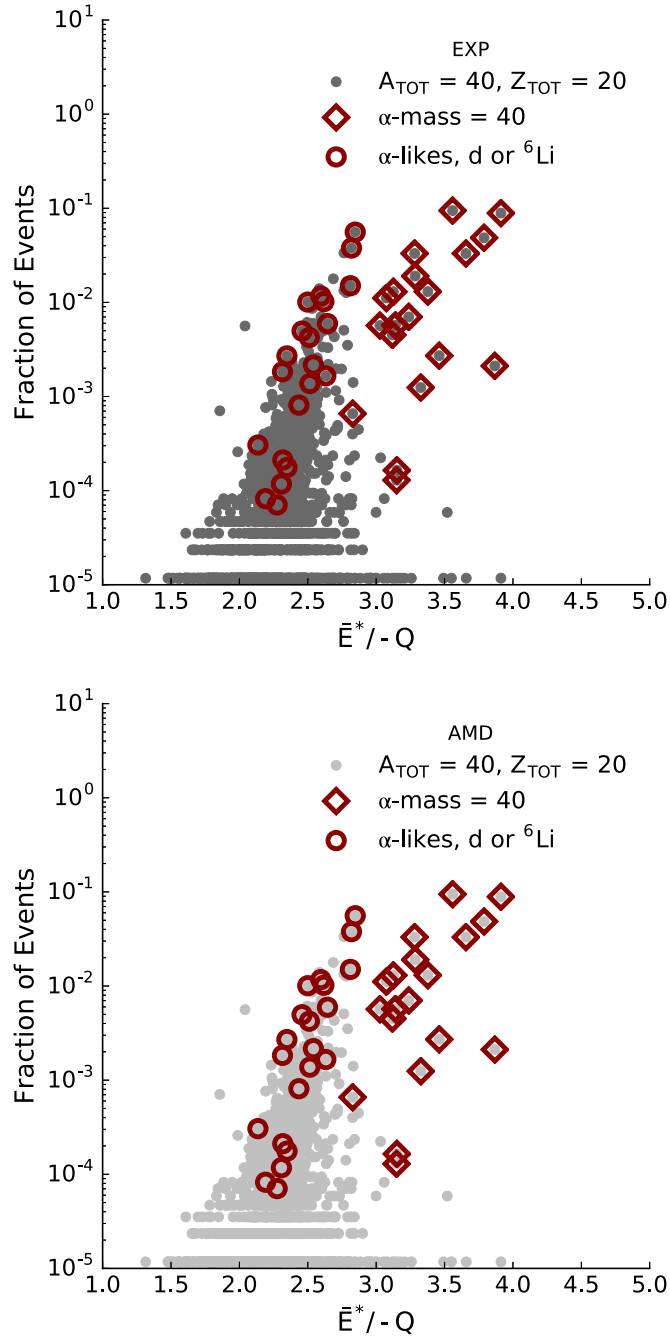

FIG. 9. The fraction of exit channel events as a function of the ratio of the average excitation energy to the separation energy. Top panel shows experimental data, bottom panel shows AMD calculation. Each solid circle represents an exit channel. The $A_L = 40$ channels are identified by using large open diamonds. Events identified by open circles may be $A_L = 40$ channels which have undergone secondary decays with d and ^{6}Li emissions (see text).

of the momentum flow during the decay. In the rest of Fig. 10 we present the experimental sphericity-coplanarity plots for the $A_L = 40$ exit channels. We do not include the channels with only two α-conjugate fragments which would necessarily appear at 0.0 in the sphericity-coplanarity plane. Most exit channel event distributions fall closer to the coplanar region of

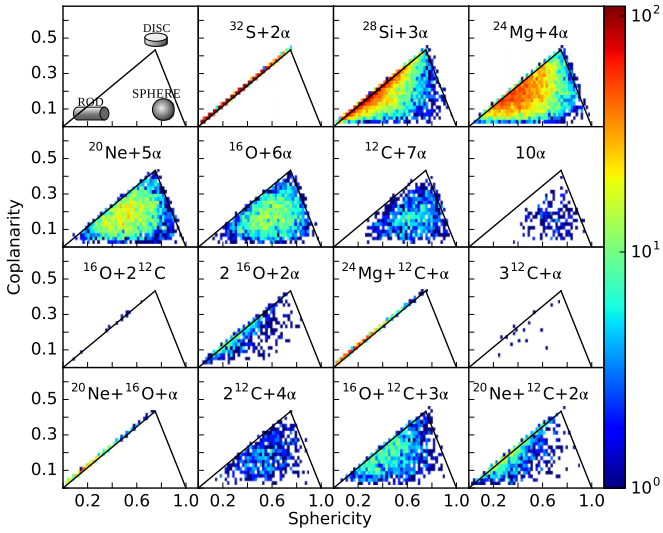

FIG. 10. Sphericity coplanarity plots for the $A_L = 40$ exit channels. Two-body exit channels are excluded. See text.

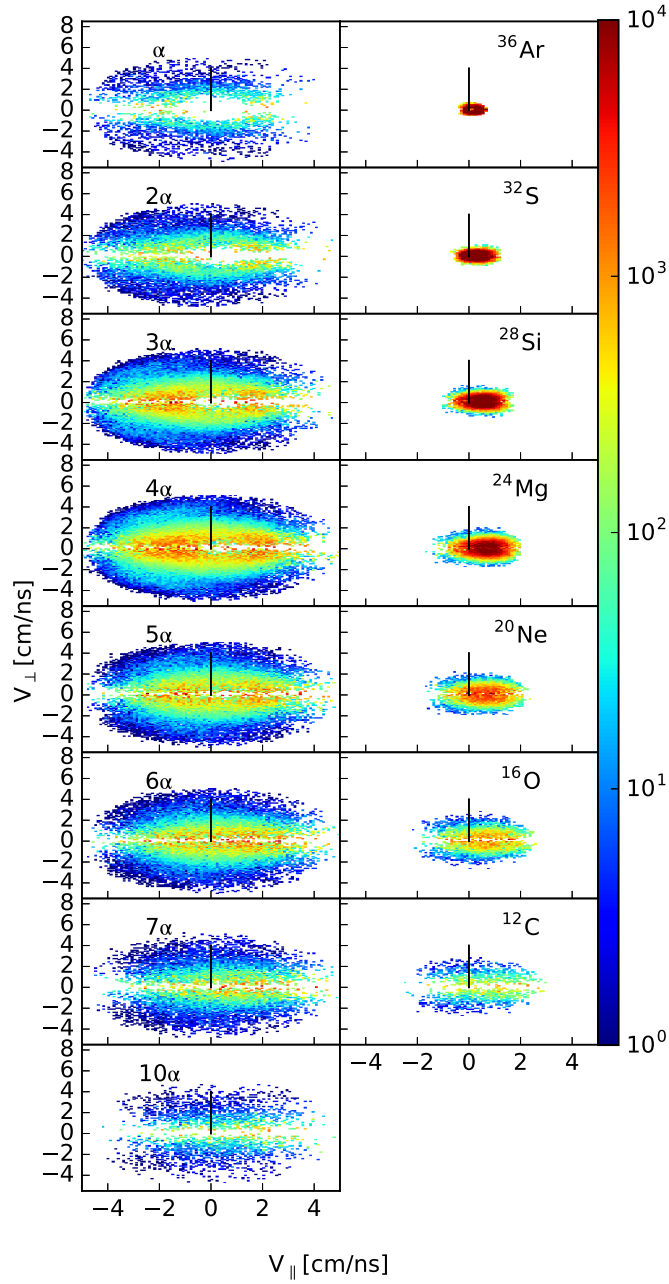

FIG. 11. Source-frame-invariant velocity plots for the α-like exit channels containing α particles. Vertical lines at 0 are to aid the eye in comparisons of these distributions.

the rod to disk axis than that of the sphere and only the larger multiplicity events approach the latter. In some previous work similar observations have been attributed to multiplicity effects [43]. While it is obvious that fluctuations will be important and that two- and three-fragment events will necessarily be coplanar in this representation, in general, the distribution will reflect the initial momentum distribution resulting from the collision as well as the mode and sequence of subsequent deexcitations and momentum conservation in that sequence, rather than the multiplicity, per se. The generally prolate nature of the sphericity-coplanarity plots of Fig. 10 suggest that the exit channels with large numbers of α particles result from processes in which an initial breakup into larger excited fragments is followed by α-particle deexcitation. Under very specific circumstances of simultaneous fragmentation, the observed momentum space shape should be more directly related to the initial geometric configuration of the deexciting system [44].

To understand these $A_L = 40$ events in more detail, we have constructed invariant velocity distributions for the single fragment ($x\alpha$) exit channels, Fig. 11, and the two-fragment exit channels, Fig. 12. The products of the different decay channels are transformed into the rest frame of the reconstructed α-like mass 40 nucleus. The decay channels are indicated in the various panels. The vertical lines indicate the rest-frame parallel velocity of the reconstructed emitting source. In these figures the right-hand panels show the invariant velocity distributions for the heaviest fragment in the event and the left-hand panels show the invariant velocity distribution for the α particles or other remnants of the deexcitation. In Fig. 11 we note that the velocity spectra of the heaviest fragment is peaked at a parallel velocity above the reconstructed source velocity while the α-particle velocities are centered at lower parallel velocities than the reconstructed source velocity. We also note that the α-particle velocity distributions become more symmetric about the source velocity as the multiplicity of α particles increases. In Fig. 12 we show the decay channels of α-like mass 40 nuclei which consist of pairs of heavier α-like mass fragments. Except for the symmetric two-^{20}Ne channel, we observe a similar behavior—the heavier-fragment velocities are centered at velocities larger than the velocity of the decaying nucleus while the velocity distributions for the lighter fragments peak at parallel velocities smaller than the parallel velocity of the decaying nucleus.

To emphasize the generality of this observation for the $A_L = 40$ exit channels, we show distributions of observed mass vs parallel velocity for all the different decay channels in Fig. 13. We note again in this figure that the heaviest fragment

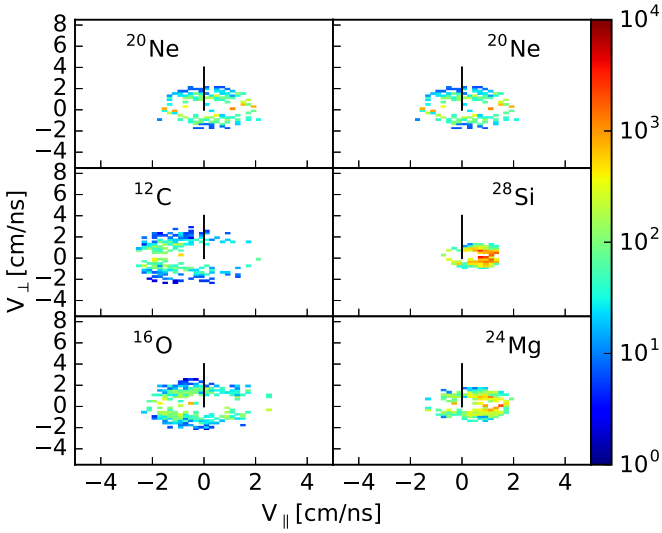

FIG. 12. Source-frame-invariant velocity plots for the two-fragment α-like exit channels. Vertical lines at 0 are to aid the eye in comparisons of these distributions.

in the different decay channels always tends to be observed at velocities larger than that of the neck region and that light particles tend to be observed as originating from the velocity region between the source velocity and the c.m. velocity, i.e., from a neck region. To verify that the effect is real and not the result of some biasing by the experimental acceptance of NIMROD, we have done statistical model calculations using the statistical deexcitation code GEMINI. When these events were filtered through our experimental acceptance the resultant parallel velocity distributions remained symmetric about the source velocity. In the present case these necks exhibit important α-clustering effects. The manifestation of this neck can be either a single α-conjugate fragment or one or more α particles either independently formed or derived from the deexcitation of an excited α-conjugate precursor. The observed emission patterns, in which the lighter fragments trail the heavier fragments, are strongly reminiscent of the "hierarchy" effect reported for other systems in a similar energy range [33,34]. It reflects a dynamics in which mass and velocity are correlated such that, for fragments emitted forward in the center of mass, the heaviest fragments are emitted at forward angles and are on average the fastest ones, the second-heaviest fragment is the second fastest one, and so on. Such behavior is inconsistent with production of a fully equilibrated compound nucleus. Rather, it signals a binary nature of the reaction with neck formation between the quasiprojectile and the quasitarget [34,35]. The breakup of this neck is fast enough that memory of the neck geometry is retained. Of course these emissions from the neck region are subject to possible modification by proximity effects [45–49].

The results in Figs. 11–13 suggest that the α particles in $x\alpha$ events observed in the left panels of Fig. 11 could originate from the same process as the fragments seen in the left-hand side of Fig. 12. As previously noted, the ^{40}Ca + ^{12}C reaction at 25 MeV/nucleon populates excited states of ^{12}C nuclei which decay by 3α emission, primarily in a sequential manner [16]. It is reasonable to expect that similar excited α deexciting states are produced in the present reaction. Indeed, we have already noted that the sphericity-coplanarity plots of Fig. 10 suggest that the exit channels with large numbers of α particles result from processes in which an initial breakup into larger excited fragments is followed by α-particle deexcitation. Further evidence for such precursors is found in our data

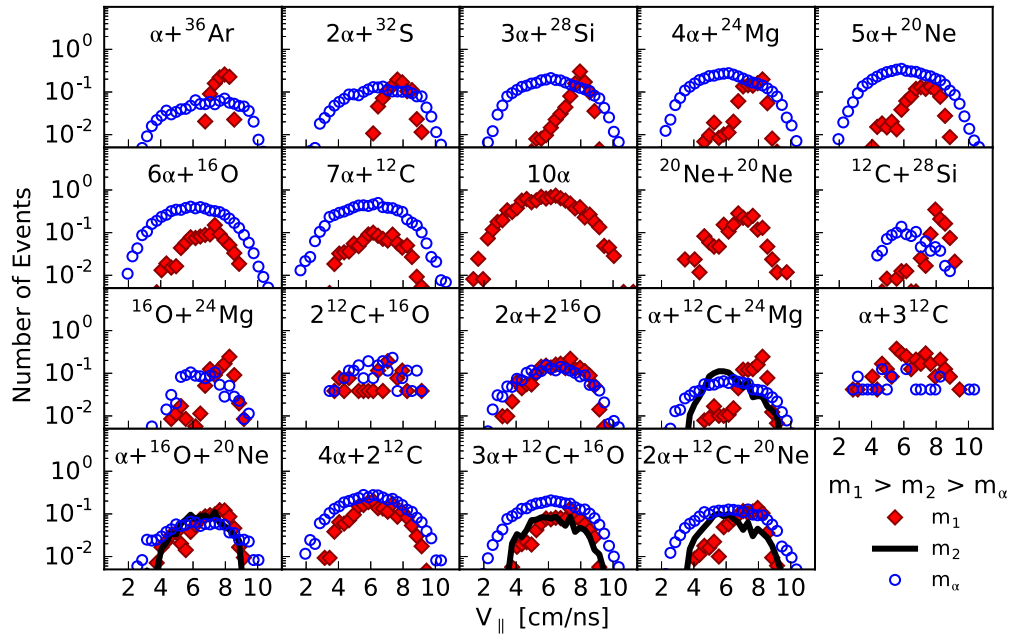

FIG. 13. Parallel velocity distributions for the α-conjugate exit channels. In each panel, distributions are color coded for different products. Solid red diamonds are for the heaviest fragment in the event, black lines are for the second-heaviest fragment, open blue circles are for α particles.

in the large numbers of ^{8}Be nuclei emitted. The granularity of the detector in our experiment is such that most of these are observed as two α particles simultaneously striking a single detector and identified by their combined ΔE, E signal. The granularity of our detector is not well suited to measuring the ^{8}Be correlation function so we do not pursue this question further.

IX. SUMMARY AND CONCLUSIONS

Reactions of 35 MeV/nucleon ^{40}Ca with ^{40}Ca have been investigated with an emphasis on peripheral and midperipheral collisions leading to excited projectile-like fragments. A global analysis of the deexcitation channels of $A = 40$ PLF fragments agrees with previous studies that total equilibration of all degrees of freedom is not achieved in the midperipheral collisions. A hierarchy effect is observed in the collision dynamics. The selection of the subset of $A = 40$ projectile-like fragment exit channels characterized by a total α-conjugate mass (α particles plus α-conjugate fragments) equal to 40 indicates that these projectile-like exit channels generally have important dynamic contributions. Most of the α particles observed in such events trail larger α-conjugate leading fragments and originate from α-conjugate neck structures formed during the collisions. The manifestation of this neck can be a single α-conjugate fragment or one or more α particles either independently formed or derived from the deexcitation of an excited α-conjugate precursor. This mechanism significantly increases the difficulty of isolating clean projectile decay samples [49].

Transport model calculations typically indicate that the neck structures formed in midperipheral collisions have densities lower than normal density [34]. Lowering of the density is expected to favor α clustering. By using a constrained Hartree–Fock–Bogoliubov approach, Girod and Schuck have explored the nuclear equation of state for self-conjugate $N = Z$ nuclei and concluded that those nuclei will cluster into a metastable phase of α particles (or in some cases α-conjugate light clusters) at excitations above 3 MeV/nucleon and densities below 0.33 normal density [50]. We believe that the reaction dynamics observed in this paper can provide a natural entry point to study the disassembly of α-clustered systems with potentially exotic geometries and properties.

ACKNOWLEDGMENTS

This work was supported by the United States Department of Energy under Grant No. DE-FG03- 93ER40773 and by The Robert A. Welch Foundation under Grant No. A0330. We appreciated the useful conversations with S. Shlomo. S. Umar, and A. Ono. We also greatly appreciate the continued excellent work of the staff of the Texas A&M University Cyclotron Institute.

[1] C. Beck, *Clusters in Nuclei* (Springer-Verlag, Berlin, Heidelberg, 2010), Vol. 1; (2012), Vol. 2; (2014), Vol 3.
[2] K. Ikeda, N. Takigawa, and H. Horiuchi, Prog. Theor. Phys. Suppl. **E68**, 464 (1968).
[3] M. Freer, Rep. Prog. Phys. **70**, 2149 (2007).
[4] W. von Oertzen, M. Freer, and Y. Kanada-Enyo, Phys. Rep. **432**, 43 (2006).
[5] Y. Kanada-En'yo and H. Horiuchi, Prog. Theor. Phys. Suppl. **142**, 205 (2001).
[6] E. Epelbaum, H. Krebs, T. A. Lähde, D. Lee, and Ulf-G. Meißner, Phys. Rev. Lett. **109**, 252501 (2012).
[7] E. Johnson, G. Rogachev, V. Goldberg, S. Brown, D. Robson, A. Crisp, P. Cottle, C. Fu, J. Giles, B. Green *et al.*, Eur. Phys. J. A **42**, 135 (2009).
[8] T. Fukui, Y. Taniguchi, T. Suhara, Y. Kanada-En'yo, and K. Ogata, Phys. Rev. C **93**, 034606 (2016).
[9] Y. Funaki, T. Yamada, H. Horiuchi, G. Röpke, P. Schuck, and A. Tohsaki, Phys. Rev. Lett. **101**, 082502 (2008).
[10] A. Tohsaki, H. Horiuchi, P. Schuck, and G. Röpke, Phys. Rev. Lett. **87**, 192501 (2001).
[11] G. Röpke, A. Schnell, P. Schuck, and P. Nozieres, Phys. Rev. Lett. **80**, 3177 (1998).
[12] A. S. Umar, J. A. Maruhn, N. Itagaki, and V. E. Oberacker, Phys. Rev. Lett. **104**, 212503 (2010).
[13] S. Hamada, Y. Hirabayashi, N. Burtebayev, and S. Ohkubo, Phys. Rev. C **87**, 024311 (2013).
[14] N. T. Zinner and A. S. Jensen, J. Phys. G **40**, 053101 (2013).
[15] P. E. Hodgson and E. Běták, Phys. Rep. **374**, 1 (2003).
[16] A. R. Raduta, B. Borderie, E. Geraci, N. Le Neindre, P. Napolitani, M. Rivet, R. Alba, F. Amorini, G. Cardella, M. Chatterjee *et al.*, Phys. Lett. B **705**, 65 (2011).
[17] J. Manfredi, R. J. Charity, K. Mercurio, R. Shane, L. G. Sobotka, A. H. Wuosmaa, A. Banu, L. Trache, and R. E. Tribble, Phys. Rev. C **85**, 037603 (2012).
[18] O. S. Kirsebom, M. Alcorta, M. Borge, M. Cubero, C. A. Diget, L. M. Fraile, B. R. Fulton, H. O. U. Fynbo, D. Galaviz, B. Jonson *et al.*, Phys. Rev. Lett. **108**, 202501 (2012).
[19] L. Quattrocchi, L. Acosta, F. Amorini, A. Anzalone, L. Auditore, I. Berceanu, G. Cardella, A. Chbihi, E. De Filippo, D. Dell'Aquila *et al.*, EPJ Web Conf. **117**, 07020 (2016).
[20] B. Borderie, A. R. Raduta, G. Ademard, M. Rivet, E. De Filippo, E. Geraci, N. Le Neindre, R. Alba, F. Amorini, G. Cardella *et al.*, Phys. Lett. B **755**, 475 (2016).
[21] P. Marini, H. Zheng, M. Boisjoli, G. Verde, A. Chbihi, P. Napolitani, G. Ademard, L. Augey, C. Bhattacharya, B. Borderie *et al.*, Phys. Lett. B **756**, 194 (2016).
[22] H. Zheng and A. Bonasera, Phys. Rev. C **86**, 027602 (2012).
[23] H. Zheng, G. Giuliani, and A. Bonasera, Phys. Rev. C **88**, 024607 (2013).
[24] G. J. Mathews, B. G. Glagola, R. A. Moyle, and V. E. Viola, Jr., Phys. Rev. C **25**, 2181 (1982).
[25] S. Wuenschel, K. Hagel, R. Wada, J. Natowitz, S. Yennello, Z. Kohley, C. Bottosso, L. May, W. Smith, D. Shetty *et al.*, Nucl. Instrum. Methods Phys. Res., Sect. A **604**, 578 (2009).
[26] K. Hagel, R. Wada, J. Cibor, M. Lunardon, N. Marie, R. Alfaro, W. Shen, B. Xiao, Y. Zhao, Z. Majka *et al.*, Phys. Rev. C **62**, 034607 (2000).

[27] J. Wang, R. Wada, T. Keutgen, K. Hagel, Y. Ma, M. Murray, L. Qin, A. Botvina, S. Kowalski, T. Materna *et al.*, Phys. Rev. C **72**, 024603 (2005).
[28] A. Ono, Phys. Rev. C **59**, 853 (1999).
[29] A. Ono, EPJ Web Conf. **122**, 11001 (2016).
[30] R. Charity, M. McMahan, G. Wozniak, R. McDonald, L. Moretto, D. Sarantites, L. Sobotka, G. Guarino, A. Pantaleo, L. Fiore *et al.*, Nucl. Phys. A **483**, 371 (1988).
[31] K. Hagel, M. Gonin, R. Wada, J. Natowitz, F. Haddad, Y. Lou, M. Gui, D. Utley, B. Xiao, J. Li *et al.*, Phys. Rev. C **50**, 2017 (1994).
[32] Y. Larochelle, L. Beaulieu, G. Anctil, B. Djerroud, D. Doré, R. Laforest, J. Pouliot, R. Roy, M. Samri, C. St-Pierre *et al.*, Phys. Rev. C **53**, 823 (1996).
[33] J. Colin, D. Cussol, J. Normand, N. Bellaize, R. Bougault, A. Buta, D. Durand, O. Lopez, L. Manduci, J. Marie *et al.*, Phys. Rev. C **67**, 064603 (2003).
[34] V. Baran, M. Colonna, and M. Di Toro, Nucl. Phys. A **730**, 329 (2004).
[35] Y. Larochelle, L. Gingras, L. Beaulieu, X. Qian, Z. Saddiki, B. Djerroud, D. Doré, R. Laforest, R. Roy, M. Samri *et al.*, Phys. Rev. C **55**, 1869 (1997).
[36] R. Wada, T. Keutgen, K. Hagel, Y. Ma, J. Wang, M. Murray, L. Qin, P. Smith, J. Natowitz, R. Alfarro *et al.*, Phys. Rev. C **69**, 044610 (2004).
[37] H. Fuchs and K. Mohring, Rep. Prog. Phys. **57**, 231 (1994).
[38] D. Horn, G. Ball, D. Bowman, A. Galindo-Uribarri, E. Hagberg, R. Laforest, J. Pouliot, and R. Walker, *Advances in Nuclear Dynamics* (Springer, 1996), pp. 105–112.
[39] L. Beaulieu, R. Laforest, J. Pouliot, R. Roy, C. St-Pierre, G. Ball, E. Hagberg, D. Horn, and R. Walker, Nucl. Phys. A **580**, 81 (1994).
[40] H. Horiuchi and K. Ikeda, Prog. Theor. Phys. **40**, 277 (1968).
[41] Y. Larochelle, C. St-Pierre, L. Beaulieu, N. Colonna, L. Gingras, G. Ball, D. Bowman, M. Colonna, G. D'Erasmo, E. Fiore *et al.*, Phys. Rev. C **59**, R565(R) (1999).
[42] G. Fái and J. Randrup, Nucl. Phys. A **404**, 551 (1983).
[43] J. Bondorf, C. Dasso, R. Donangelo, and G. Pollarolo, Phys. Lett. B **240**, 28 (1990).
[44] R. Najman, R. Płaneta, A. Sochocka, F. Amorini, L. Auditore, T. Cap, G. Cardella, E. De Filippo, E. Geraci, A. Grzeszczuk *et al.*, Phys. Rev. C **92**, 064614 (2015).
[45] R. Charity, L. Sobotka, N. Robertson, D. Sarantites, J. Dinius, C. Gelbke, T. Glasmacher, D. Handzy, W. Hsi, M. Huang *et al.*, Phys. Rev. C **52**, 3126 (1995).
[46] S. Hudan, R. Alfaro, L. Beaulieu, B. Davin, Y. Larochelle, T. Lefort, V. Viola, H. Xu, R. Yanez, R. de Souza *et al.*, Phys. Rev. C **70**, 031601 (2004).
[47] S. Hudan, R. T. de Souza, and A. Ono, Phys. Rev. C **73**, 054602 (2006).
[48] A. B. McIntosh, S. Hudan, C. J. Metelko, R. T. de Souza, R. J. Charity, L. G. Sobotka, W. G. Lynch, and M. B. Tsang, Phys. Rev. Lett. **99**, 132701 (2007).
[49] C. Montoya, W. Lynch, D. Bowman, G. F. Peaslee, N. Carlin, R. De Souza, C. Gelbke, W. Gong, Y. Kim, M. Lisa *et al.*, Phys. Rev. Lett. **73**, 3070 (1994).
[50] M. Girod and P. Schuck, Phys. Rev. Lett. **111**, 132503 (2013).